FDTD Maxwell's Equations Models for Nonlinear Electrodynamics and Optics

Rose M. Joseph, *Member, IEEE* and Allen Taflove, *Fellow, IEEE*

Invited Paper

***Abstract*—This paper summarizes algorithms which extend the finite-difference time-domain (FDTD) solution of Maxwell's equations to nonlinear optics. The use of FDTD in this field is novel. Previous modeling approaches were aimed at modeling optical-wave propagation in electrically long structures such as fibers and directional couplers, wherein the primary flow of energy is along a single principal direction. However, FDTD is aimed at modeling compact structures having energy flow in arbitrary directions. Relative to previous methods, FDTD achieves robustness by directly solving, for fundamental quantities, the optical E and H fields in space and time rather than performing asymptotic analyses or assuming paraxial propagation and nonphysical envelope functions. As a result, it is almost completely general. It permits accurate modeling of a broad variety of dispersive and nonlinear media used in emerging technologies such as micron-sized lasers and optical switches.**

***Index Terms*—FDTD methods, nonlinear wave propagation.**

I. Introduction

TODAY'S need for faster and better means of communication and data processing has encouraged rapid growth of the field of nonlinear optics. This has led to development of a variety of new devices for transmitting, switching, and storing data using electromagnetic energy in and near the visible spectrum. These devices include optical fibers, couplers, switches, and amplifiers. Materials technology and fabrication methods, particularly for semiconductors, have advanced accordingly, allowing devices to be built on a submicron scale with fine structural details. Pulses as fast as a few tens of femtoseconds are being generated and guided through these new systems at repetition rates approaching the terahertz regime.

One result of this progress is the increased need for accurate models for predicting the electromagnetic field behavior of these new optical devices to permit their efficient design without repeatedly building expensive prototypes. Fortunately, the tremendous increase in computing power has made detailed numerical modeling available to the optical-design engineer. An emerging modeling tool in this area is the finite-difference time-domain (FDTD) solution of Maxwell's equations [1]–[3]. While FDTD is now well accepted in the analysis of linear electromagnetic problems, especially at microwave frequencies, it is still a novel approach in the nonlinear optics community that has long used asymptotic and paraxial wave equation models derived from Maxwell's equations as the primary detailed modeling tool. As this paper will show, the full-wave time-domain features of the FDTD field solver, augmented by recent extensions, are particularly well-suited to bring new insight to nonlinear optics problems.

To observe nonlinear effects in commonly used materials, a high-intensity light source, such as a laser, is required. The nonlinear behavior is due to the dependence of the polarization $P(t)$ on the applied electric field, $E(t)$. Assuming an isotropic and frequency-independent medium, the polarization can be expanded as a power series in E [4]

$$\begin{aligned} P &= \varepsilon_0 \left[\chi^{(1)}E + \chi^{(2)}E^2 + \chi^{(3)}E^3 + \cdots\right] \\ &= P^L + P^{NL} \end{aligned} \tag{1}$$

where P^L and P^{NL} are, respectively, the linear and nonlinear components of the polarization. Here, $\chi^{(1)}$ denotes the linear susceptibility of the medium, and the quantities $\chi^{(2)}$, $\chi^{(3)}$, $\cdots$ are the nonlinear susceptibilities. The particular nonlinear effect observed depends on which term is dominant in (1). Second- and third-order nonlinear behavior, requiring less input power to observe than higher order effects, have been the topic of much study. Some second-order nonlinear effects include sum and difference frequency generation, parametric amplification, and the Pockels effect [5]. $\chi^{(2)}$ disappears for materials with inversion symmetry such as optical-fiber glass. In such materials, the lowest order nonlinear coefficient is $\chi^{(3)}$. Third-order nonlinear effects include the quadratic electro-optic effect, third-harmonic generation, four-wave mixing, intensity-dependent refractive index, stimulated Raman and Brillouin scattering, and two-photon absorption [5]. In most optical materials, the refractive index n also varies with frequency resulting in both linear and nonlinear chromatic dispersion.

Both analytical and numerical methods have been applied to model the behavior of light propagating in a nonlinear medium.

Manuscript received May 8, 1996; revised October 10, 1996. This work was supported in part by NSF Grant ECS-9218494, ONR Contract N00014-93-0133, NASA-Ames University Consortium Joint Research Interchanges NCA2-561, 562 and 727, and Cray Research, Inc.

R. M. Joseph is with the MIT Lincoln Laboratory, Lexington, MA 02173 USA.

A. Taflove is with the Department of Electrical and Computer Engineering, McCormick School of Engineering, Northwestern University, Evanston, IL 60208 USA.

Publisher Item Identifier S 0018-926X(97)02286-2.

Typical approaches begin with a wave equation

$$\nabla^2 E - \mu_0 \varepsilon_0 \varepsilon_r(x, y, z, \omega, E) \frac{\partial^2 E}{\partial t^2} = 0 \tag{2}$$

derived from Maxwell's equations, where the relative permittivity ε_r can be spatially varying, frequency dependent, and nonlinear in E. Here, the divergence of the electric field is assumed to be negligible. The linear and nonlinear contributions of E to the polarization can be treated separately to obtain

$$\nabla^2 E - \mu_0 \varepsilon_0 n_0^2 \frac{\partial^2 E}{\partial t^2} = \mu_0 \frac{\partial^2 P^{NL}}{\partial t^2} \tag{3}$$

where n_0 is the linear refractive index and $\partial^2 P^{NL}/\partial t^2$ comprises the nonlinear term of interest.

Here, most models for nonlinear optical processes make any of several assumptions. First, a preferred direction of energy transport may be assumed. In guided-wave problems, the transverse modal profile may be decoupled from the propagation equation. Second, the variation of the electric-field envelope $\tilde{E}$ may be assumed to be small over distances of the order of one optical wavelength. This *slowly varying envelope approximation* (SVEA) permits second derivatives of $\tilde{E}$ in the propagation direction to be neglected, reducing the wave equation of (3) to a simpler propagation equation [6]. Such simplified models may have analytical or numerical solutions that permit effective simulation of optical-pulse propagation over very long distances [6], [7]. An example where this is required is long-distance pulse propagation in a single-mode fiber, where signals can travel many hundreds of kilometers. Here, the transverse (modal) profile of the light in the fiber remains constant, reducing the problem to one spatial dimension. The reduced-order equation can then be transformed to a reference frame that travels with the pulse $T = t - \beta z$, where β is the propagation constant [6]. The most common case of this method results in the *nonlinear Schrödinger equation* (NLSE), which is used to study pulse propagation in a $\chi^{(3)}$ medium

$$j \frac{\partial \tilde{E}}{\partial z} = \frac{1}{2} \beta_2 \frac{\partial^2 \tilde{E}}{\partial T^2} - \gamma |\tilde{E}|^2 \tilde{E}. \tag{4}$$

Here, β_2 is the group velocity dispersion and γ is the nonlinear coefficient. For an optical pulse propagating in a fiber, for example, the first term of (4) gives the propagation behavior, the second term accounts for the pulse spreading due to linear dispersion, and the third term models the third-order nonlinearity. For a very short pulse having a spectral width comparable to its center frequency, cubic and higher order dispersion effects become appreciable, and the NLSE model of (4) is inadequate. Additional terms must be included to model such higher order behavior [6]. Reference [8] showed that a suitable NLSE model can accurately predict the behavior of pulses as short as 10–15 optical cycles for one-dimensional (1-D) propagation problems.

Clearly, optical fibers are designed such that the transverse mode is well confined and radiation losses are low. However, for wave propagation that is not totally confined in the transverse direction, the possibility exists for transverse energy flow. Consider, for example, the case of optical-beam propagation in a bulk, nonlinear $\chi^{(3)}$ material. Here, by applying the *paraxial approximation* (which assumes that the beam energy does not diverge much from its primary direction of propagation [9]), an NLSE model analogous to (4) can be constructed wherein the second term in the equation represents transverse beam diffraction rather than longitudinal pulse dispersion. Note, however, that the assumption of paraxial propagation fundamentally limits such NLSE models to predictions of small-angle scattering or diffraction loss.

In contrast, the numerical FDTD method for nonlinear optics is completely general. FDTD is an explicit full-wave finite-difference solution of the time-dependent Maxwell's equations that yields both electric and magnetic fields with a spatial resolution much finer than one wavelength. As a result, FDTD typically requires tens of Mwords and tens of thousands of time steps of solution evolution to solve practical problems in modern nonlinear optics. However, the results often justify the computational burden since the number of approximations made is minimized and detailed field solutions are provided with an accuracy determined primarily by the grid resolution. In fact, for many of today's compact optical devices, which span just a few optical wavelengths, the computational requirements of FDTD are not prohibitive. In the following sections, we review selected algorithms for modeling nonlinear optical physics via FDTD. The algorithms allow prediction of the optical-field dynamics in complicated optical structures in the presence of material dispersions of arbitrary order and both instantaneous and time-dependent nonlinearities.

II. An Algorithm for Linear Dispersion Adaptable to Nonlinear Dispersive Optical Materials

Consider for simplicity a 1-D problem with electric and magnetic field components E_z and H_y propagating in the x direction. Assuming first that the medium is linear, nonpermeable, isotropic, and nondispersive, Maxwell's curl equations in one dimension are

$$\frac{\partial H_y}{\partial t} = \frac{1}{\mu_o} \frac{\partial E_z}{\partial x} \tag{5a}$$

$$\frac{\partial D_z}{\partial t} = \frac{\partial H_y}{\partial x} \tag{5b}$$

where μ_o = vacuum permeability, $D_z = \varepsilon E_z$, and the permittivity ε is independent of frequency. Using Yee's central differencing in time and space [1], these relations can be expressed as

$$H_y|_{i+1/2}^{n+1/2} = H_y|_{i+1/2}^{n-1/2} + \frac{\Delta t}{\mu_o \Delta x} (E_z|_{i+1}^{n} - E_z|_{i}^{n}) \tag{6a}$$

$$D_z|_{i}^{n+1} = D_z|_{i}^{n} + \frac{\Delta t}{\Delta x} (H_y|_{i+1/2}^{n+1/2} - H_y|_{i-1/2}^{n+1/2}) \tag{6b}$$

$$E_z|_{i}^{n+1} = \frac{1}{\varepsilon_i} D_z|_{i}^{n+1} \tag{6c}$$

and the solution iterated to the desired final observation time. For a general dispersive and nonlinear medium, however, the FDTD computational model can retain its fully explicit nature if (6c) is replaced by the constitutive relation

$$E_z|_{i}^{n+1} = f(D_z|_{i}^{n+1}, D_z|_{i}^{n}, \cdots; E_z|_{i}^{n}, E_z|_{i}^{n-1}, \cdots) \tag{7}$$

where f is a function to be determined. Several approaches have been proposed for this purpose. These may be categorized into two primary groups: recursive-convolution methods [3], [10]–[12] and the direct time integration methods [2], [13]–[15]. An advantage of the direct time integration methods is that they can be generalized to nonlinear dispersive materials. This section summarizes a direct time integration method shown to be adaptable to nonlinear optical modeling [2].

We now consider a linear dispersive material characterized by N Lorentzian resonances. For each vector component of $\vec{D}$ and $\vec{E}$, we write

$$D(\bar{r}, t) = \varepsilon_o E(\bar{r}, t) + P(\bar{r}, t). \tag{8}$$

Here, the polarization of an electric-field vector component is expressed as a sum of N terms (dropping the vector component subscript for simplicity)

$$P = \sum_{i=1}^{N} P_i \tag{9}$$

where each P_i term is a convolution integral

$$P_i = \varepsilon_o \int_0^t \chi_i(t-\tau) E(\tau)\, d\tau \tag{10}$$

and each χ_i is a Lorentzian in frequency

$$\chi_i(\omega) = \frac{G_i \omega_i^2 (\varepsilon_S - \varepsilon_\infty)}{\omega_i^2 + 2j\omega\delta_i - \omega^2}$$

with

$$\sum_{i=1}^{N} G_i = 1. \tag{11}$$

In (10), we assume zero values of the electric field and the kernel functions for $t \leq 0$.

Now consider the key property that drives this formulation, namely, each kernel function $\chi_i(t)$ satisfies the following linear, second-order differential equation:

$$\chi_i'' + 2\delta_i \chi_i' + \omega_i^2 \chi_i = 0 \tag{12}$$

where it is assumed that and $\chi_i(t=0) = 0$ and $\chi_i'(t=0) = G_i\omega_i^2(\varepsilon_S - \varepsilon_\infty)$. This property of the kernel function makes it possible to treat the convolution integral as a new dependent variable. It follows immediately that a second-order ordinary differential equation can be derived for the linear convolution integral by time-differentiating it. This equation determines the polarization which can then be used to determine E. Knowing

$$E = \frac{1}{\varepsilon_\infty \varepsilon_o}\left(D - \sum_{i=1}^{N} P_i\right) \tag{13}$$

we can write for each convolution integral P_i the differential equation

$$P_i'' + 2\delta_i P_i' + \omega_i^2 P_i = \omega_i^2 b_i \left(D - \sum_{i=1}^{N} P_i\right)$$

where

$$b_i = G_i(\varepsilon_S - \varepsilon_\infty). \tag{14}$$

As an example of the application of (14), consider the case of a material having three Lorentzian relaxations. This results in the following system of ordinary differential equations:

$$P_1'' + 2\delta_1 P_1' + \omega_1^2(1+b_1)P_1 + \omega_1^2 b_1 P_2 + \omega_1^2 b_1 P_3 = \omega_1^2 b_1 D \tag{15a}$$

$$P_2'' + 2\delta_2 P_2' + \omega_2^2(1+b_2)P_2 + \omega_2^2 b_2 P_1 + \omega_2^2 b_2 P_3 = \omega_2^2 b_2 D \tag{15b}$$

$$P_3'' + 2\delta_3 P_3' + \omega_3^2(1+b_3)P_3 + \omega_3^2 b_3 P_1 + \omega_3^2 b_3 P_2 = \omega_3^2 b_3 D. \tag{15c}$$

Applying a second-order accurate, semi-implicit central-difference scheme centered at time step n, this system can be solved to update P_1, P_2, and P_3 by inverting the following set of equations:

$$\begin{aligned} a_1 P_1^{n+1} + c_1 P_2^{n+1} + c_1 P_3^{n+1} &= c_1(D^{n+1} + D^{n-1}) - c_1(P_2^{n-1} \\ &\quad + P_3^{n-1}) + 4P_1^n + g_1 P_1^{n-1} \end{aligned} \tag{16a}$$

$$\begin{aligned} c_2 P_1^{n+1} + a_2 P_2^{n+1} + c_2 P_3^{n+1} &= c_2(D^{n+1} + D^{n-1}) - c_2(P_1^{n-1} \\ &\quad + P_3^{n-1}) + 4P_2^n + g_2 P_2^{n-1} \end{aligned} \tag{16b}$$

$$\begin{aligned} c_3 P_1^{n+1} + c_3 P_2^{n+1} + a_3 P_3^{n+1} &= c_3(D^{n+1} + D^{n-1}) - c_3(P_1^{n-1} \\ &\quad + P_2^{n-1}) + 4P_3^n + g_3 P_3^{n-1} \end{aligned} \tag{16c}$$

where

$$a_i = 2 + 2\delta_i \Delta t + \omega_i^2 \Delta t^2 (1 + b_i); \tag{17a}$$

$$c_i = \omega_i^2 \Delta t^2 b_i \tag{17b}$$

$$g_i = -2 + 2\delta_i \Delta t - \omega_i^2 \Delta t^2 (1 + b_i). \tag{17c}$$

With the updated values P_1^{n+1}, P_2^{n+1}, and P_3^{n+1} now available, we can update E from (13) as

$$E^{n+1} = \frac{1}{\varepsilon_\infty \varepsilon_o}(D^{n+1} - P_1^{n+1} - P_2^{n+1} - P_3^{n+1}). \tag{18}$$

Equations (16)–(18) are applied in place of (7), performing the function $\{D^{n+1}\} \rightarrow \{E^{n+1}\}$. For each E component calculated in this manner, computer storage must be provided for two previous values of D and two previous values of each of the N convolution functions P_i.

The dispersive FDTD algorithm summarized above was validated in [2] by modeling the reflection of a Gaussian pulse incident on a half-space of a dispersive dielectric medium. Fig. 1 shows results for a hypothetical material having three arbitrarily chosen, moderately undamped Lorentzian resonances in the optical range. With the baseline low-frequency and high-frequency permittivities $\varepsilon_s = 10$ and $\varepsilon_\infty = 1$, the controlling parameters of the Lorentzians were assumed to be: ($f_1 = 2 \times 10^{14}$ Hz, $\delta_1 = 0.5 f_1$, $G_1 = 0.3$), ($f_2 = 4 \times 10^{14}$ Hz, $\delta_2 = 0.5 f_2$, $G_2 = 0.4$), and ($f_3 = 6 \times 10^{14}$ Hz, $\delta_3 = 0.5 f_3$, $G_3 = 0.3$). The FDTD reflection

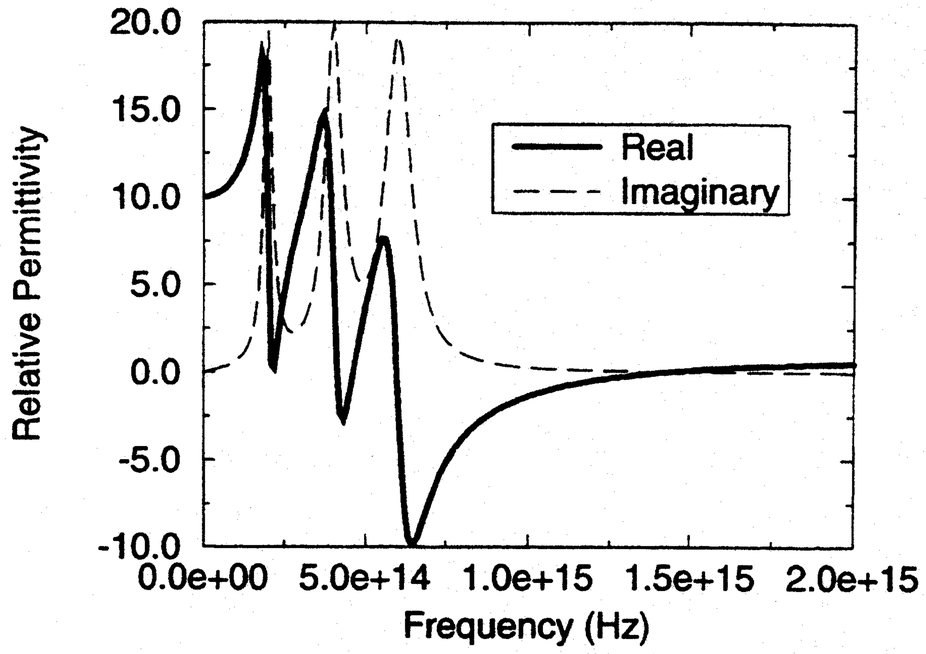

(a)

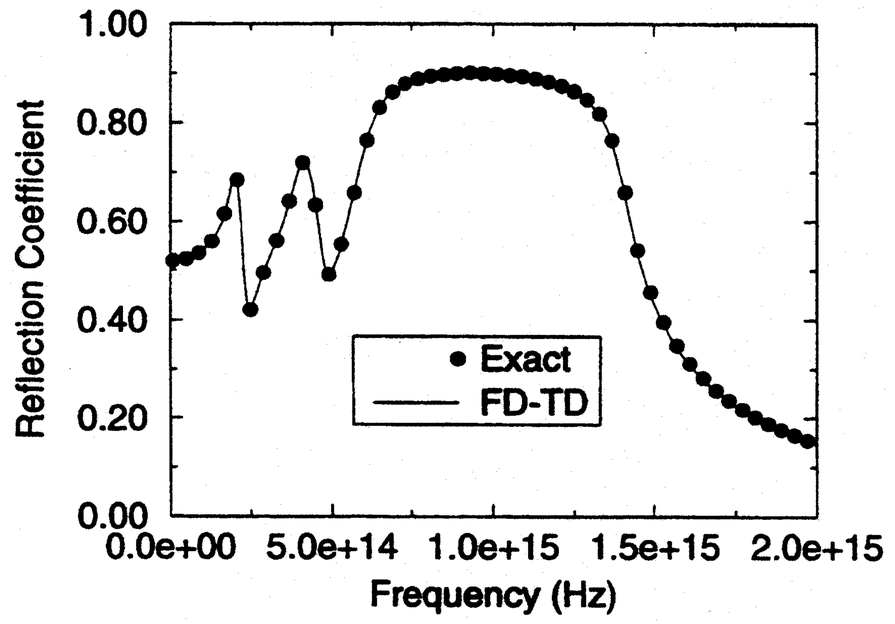

(b)

Fig. 1. (a) Real and imaginary parts of the permittivity of a Lorentz medium having three resonances in the optical range. (b) Comparison of FDTD and exact results from dc to 2.0×10^{15} Hz for the magnitude of the reflection coefficient of a half-space composed of the medium of (a). $\Delta x = 2.65$ nm, $\Delta t = 8.85$ as. Problem size: 20 000 1-D cells, 20 000 time steps. Computer resources: 0.92 MW; 1000 CPU s on a single processor of the Cray J90 [2].

coefficient versus frequency was computed by taking the ratio of the discrete Fourier transforms of the reflected and incident pulses. These data were then compared to the exact values obtained by monochromatic impedance theory. Agreement was within 0.1% at all frequency comparison points (literally, from dc to light).

In addition to the wave reflected from a dispersive half space, FDTD permits computing the pulse propagating within the dispersive medium at any space–time point. Historically, such pulse dynamics have been obtained only by asymptotic or Laplace transform analyses, classically by Sommerfeld [16] and Brillouin [17], and more recently in [18] and [19]. Of particular interest in these papers has been the delicate *precursor* fields [20] that can precede the main body of a pulse propagating in a Lorentz medium. The computation of the precursor for a single-Lorentz medium using a subset of the above algorithm is reported in [15]. Here, a sinusoidal source of frequency $f = 1.59 \times 10^{15}$ Hz was assumed located at $x = 0$ and switched on at $t = 0$ for material parameters $\varepsilon_s = 2.25$, $\varepsilon_\infty = 1$, $f_0 = 6.4 \times 10^{15}$ Hz, $\delta = 0.44 f_0$, and $G = 1$. Upon comparing the FDTD-computed Sommerfeld precursor observed at $x = 1\,\mu$m to the published asymptotic

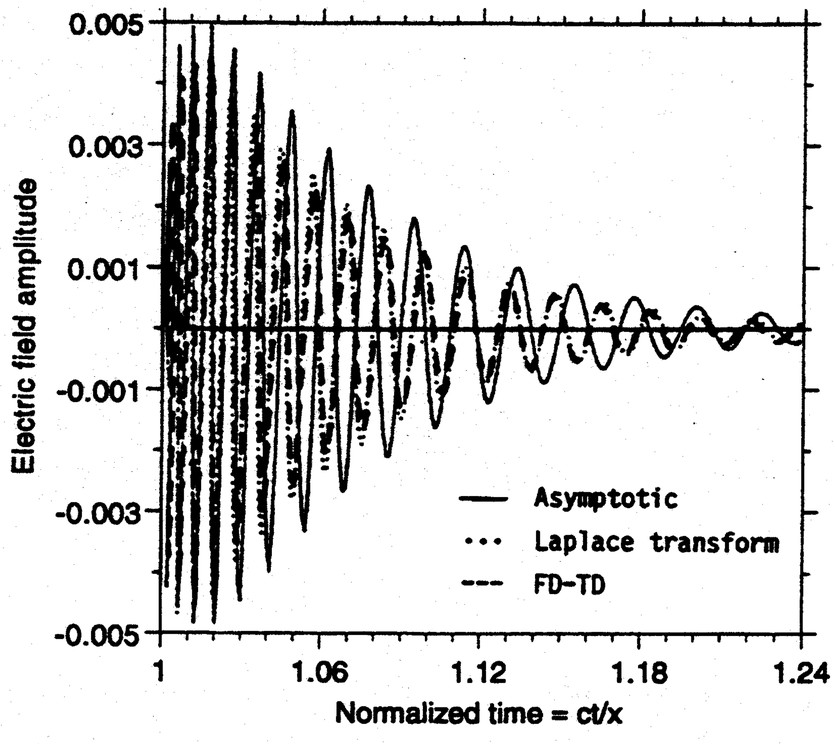

Fig. 2. Comparison of FDTD, asymptotic, and Laplace transform results for the Sommerfeld precursor observed at $x = 1\,\mu$m in a Lorentz-dispersive medium for a unit-step modulated sinusoidal excitation of $\omega_c = 1.0 \times 10^{16}$ at $x = 0$. $\Delta x = 0.0157$ nm, $\Delta t = 0.0523$ as. Problem size: 80 000 1-D cells, 80 000 time steps. Computer resources: 1.4 MW; 965 CPU s on a single processor of the Cray J90 [2].

[18] and Laplace transform [19] predictions, it was found that the FDTD precursor closely agrees with the Laplace transform calculation. This is shown in Fig. 2.

III. Third-Order Nonlinear Media

This section reviews approaches based upon the FDTD method that permit the direct time integration of Maxwell's equations for materials having third-order nonlinear behavior. In contrast to NLSE models, the optical carrier is retained. Section III-A reviews a relatively simple model of instantaneous Kerr-type nonlinearity. Section III-B reviews a much more complete model that includes simultaneous linear dispersion, instantaneous nonlinearity, and nonlinearity with a finite-time response.

A. Instantaneous Nonlinearity

The FDTD model for Kerr-type materials assumes an instantaneous nonlinear response. The nonlinearity is modeled in the relation $D = \varepsilon_0 \varepsilon E$, where

$$\begin{aligned} \varepsilon &= n^2 \\ &= (n_0 + n_2 |E|^2)^2 \\ &\simeq n_0^2 + 2 n_0 n_2 |E|^2. \end{aligned} \tag{19}$$

Here, the linear refractive index n_0 is dimensionless, and the nonlinear refractive index n_2 has units of m^2/V^2. From (19), (7) for the latest value of E can be expressed by the following iteration upon the latest value of D and the old value of E [21]:

$$E = \frac{D}{n_0^2 + 2 n_0 n_2 |E|^2}. \tag{20}$$

Knowledge of E then permits another updating of H and D, and the process repeats cyclically until time stepping is completed.

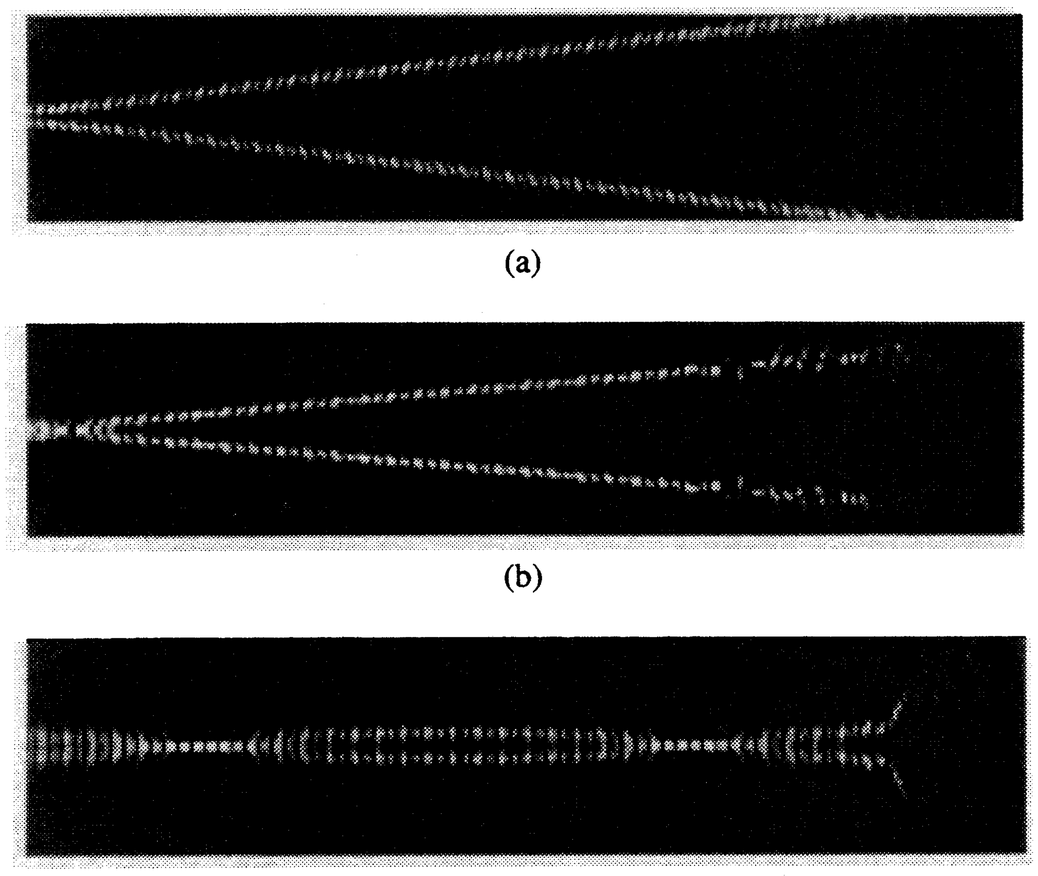

(a)

(b)

(c)

Fig. 3. Visualization of the FDTD computed electric field of optically narrow mutually interacting spatial solitons in Type-RN Corning® glass. (a) Repulsion for relative carrier phase $= \pi$. (b) Single coalescence and subsequent divergence for relative carrier phase $= 0$. (c) Periodic beam recoalescence after doubling the intensity beamwidth and separation parameters of the simulated beams, but keeping the wavelength constant. $\Delta x = \Delta y = 52.8$ nm, $\Delta t = 88.1$ as. Problem size: 1800 × 592 2-D cells, 3600 time steps. Computer resources: 10.9 MW; 1340 CPU s on a single processor of the Cray J90 [21].

The two-dimensional (2-D) FDTD modeling of *spatial optical soliton* propagation and mutual deflection in a homogeneous glass medium having a Kerr-type instantaneous third-order nonlinearity is reported in [21]. Here, the transverse spreading of a simulated laser beam caused by linear diffraction was exactly balanced by the transverse beamwidth sharpening effect due to self-focusing caused by the assumed nonlinearity. FDTD calculations were made for two parallel beams spaced at 1.05 μm, center to center. The beams were assumed to be switched on at $t = 0$ in Type-RN Corning® glass ($n_0 = 2.46$ and $n_2 = 1.25 \times 10^{-18}$ m^2/W). Each beam was assumed to have a carrier frequency of 2.31×10^{14} Hz ($\lambda = 1.3\,\mu$m), an initial hyperbolic-secant transverse profile with an intensity beamwidth (FWHM) of 0.65 μm, and an initial peak E of 6.87×10^9 V/m. The choice of these parameters yielded copropagating spatial solitons. Fig. 3(a)—taken from [21]—illustrates a mutual repulsion for a carrier phase difference of π between the beams. This is expected from the NLSE. Fig. 3(b) depicts the results for in-phase carriers. For this case, the NLSE predicts that the two beams interact by alternately attracting, coalescing, repelling, and then recoalescing. If the two beams have the appropriate amplitudes and spacing, the attraction and repulsion is periodic. In fact, [22] states that two in-phase fundamental spatial solitons having an initial field-amplitude distribution in the transverse direction of

$$A(y) = \frac{1}{kw}\left(\frac{n_0}{n_2}\right)^{1/2}\left[\operatorname{sech}\left(\frac{y-y_0}{w}\right) + \operatorname{sech}\left(\frac{y+y_0}{w}\right)\right] \tag{21}$$

oscillate in the propagation direction with a period of

$$x_p = \frac{2x_0 \sinh\left(\dfrac{2y_0}{w}\right)\cosh\left(\dfrac{y_0}{w}\right)}{\dfrac{2y_0}{w} + \sinh\left(\dfrac{2y_0}{w}\right)} \tag{22}$$

based on the NLSE theory of [23]. Here, w is the characteristic width of the hyperbolic secant, $y_0 = 1.42w$, $2y_0$ is the center-to-center separation of the two beams, and $x_0 = \pi^2 n_0 w^2/\lambda$ is the soliton period. For the choice of parameters used in the FDTD simulations of [21], the predicted repetition period was $x_p = 9\,\mu$m. However, as shown in Fig. 3(b), the FDTD calculations showed only a single beam coalescence and then subsequent beam divergence to arbitrarily large separations for an effective $x_p = \infty$.

It was a goal to understand why the FDTD Maxwell's equations model did not agree with the NLSE prediction in this case. The first possibility considered was that the FDTD simulation was flawed because of inadequate grid resolution or inadequate decoupling of the beam-interaction region from the outer-grid boundaries (second-order Mur ABC's were used at the time). In a series of exploratory modeling runs, the space–time resolution of the FDTD grid was progressively refined and the grid was progressively enlarged. These changes gave results identical to those of the original FDTD model. Therefore, the original FDTD model was concluded to be numerically converged and sufficiently free of the outer boundary artifact to yield plausible results.

The second possibility considered was that the ratio of beamwidth to wavelength was below the limit of applicability of NLSE. Because it is known that additional terms in the NLSE are required to model higher order effects for temporal solitons, it was reasoned that NLSE modeling of copropagating spatial solitons would be more physically meaningful if the two beams were widened relative to the optical wavelength, while maintaining the same ratio of beamwidth-to-beam separation. This would reduce linear beam-diffraction effects, hopefully bringing the test case into the region of validity for the simple NLSE model. To test this possibility, [21] reported two new FDTD simulations where the intensity beamwidth B_I and separation parameters of the simulated beams were each doubled and then doubled again, keeping the dielectric wavelength λ_d constant. This FDTD simulation is shown in Fig. 3(c).

After the first doubling of beamwidth and beam separation, the FDTD-predicted spatial solitons began to qualitatively show the recoalescence behavior predicted by NLSE, but with a 38% longer period of recoalescence than the NLSE value. After the second doubling, the FDTD and NLSE predictions for repetition period x_p showed much better agreement, differing by only 13%. A third data point (calculated for this paper) involved, yet again, a 50% increase in beamwidth and beam separation. This resulted in the difference between the FDTD and NLSE calculations of x_p dropping further to only 5%. Results for these numerical experiments are shown in Table I.

It was concluded that there is a strong likelihood that copropagating optically narrow spatial solitons have only a single coalescence and then indefinite separation. The FDTD model

TABLE I
PROGRESSIVE AGREEMENT OF FDTD AND NLSE RESULTS FOR PERIODICITY OF COPROPAGATING SPATIAL SOLITONS AS THE RATIO OF THE BEAMWIDTH TO WAVELENGTH INCREASES

B_I, FWHM (μm)	B_I/λ_d	x_p (μm) NLSE	x_p (μm) FDTD	Difference
0.65	1.22	9	∞	∞%
1.3	2.46	34	47	38%
2.6	4.9	135	153	13%
3.9	7.36	305	320	5%

appears to properly predict the behavior of these solitons in nonlinear media both in the regime where the standard NLSE model breaks down ($B_I/\lambda_d < 1$) and the regime where the standard NLSE model is valid ($B_I/\lambda_d \gg 1$). The paraxial approximation inherent to NLSE, according to [9], accounts only for zeroth-order linear diffraction effects. Since the FDTD model implements the fundamental Maxwell's curl equations, it makes no assumption about a preferred scattering direction. It naturally accounts for energy transport in arbitrary transverse directions and should be exact for the computed optical electromagnetic fields up to the limit set by the grid resolution. Reference [24] reported a similar need to use a full-wave Maxwell's model to properly obtain nonparaxial scattering of energy for a corrugated waveguide beam-steering device.

B. Dispersive Nonlinearity

This section reviews an algorithm reported in [25] and [26] for modeling the simultaneous presence of linear dispersion, instantaneous nonlinearity, and dispersive nonlinearity (see also [24], [27], and [28]). Consider, again, the 1-D problem of (5a) and (b). Now allow for nonlinearity of the dielectric by assuming that the electric polarization consists of two parts: a linear part P_z^L and a nonlinear part P_z^{NL} [6]. Maxwell's equations still govern, but here, E must be related to D by accounting for both the linear and nonlinear components of the polarization

$$E_z = \frac{D_z - (P_z^L + P_z^{NL})}{\varepsilon_\infty \varepsilon_o}. \tag{23}$$

Here, P_z^L is given by the convolution of $E_z(x, t)$ and the first-order susceptibility function $\chi^{(1)}$

$$P_z^L(x, t) = \varepsilon_o \int_{-\infty}^{\infty} \chi^{(1)}(t - \tau) E_z(x, \tau)\, d\tau \tag{24}$$

where $\chi^{(1)}$ provides the physics of linear dispersion normally associated with a frequency-dependent permittivity. Further, P_z^{NL} is given by the convolution of $E_z(x, t)$ and the third-order susceptibility function $\chi^{(3)}$

$$P_z^{NL}(x, t) = \varepsilon_o \int_{-\infty}^{\infty}\int_{-\infty}^{\infty}\int_{-\infty}^{\infty} \cdot \left[\begin{array}{c} \chi^{(3)}(t - \tau_1, t - \tau_2, t - \tau_3)\cdot \\ E_z(x, \tau_1) E_z(x, \tau_2) E_z(x, \tau_3)\, d\tau_1\, d\tau_2\, d\tau_3 \end{array}\right] \tag{25}$$

where $\chi^{(3)}$ provides the physics of a nonlinearity with retardation or memory (i.e., a dispersive nonlinearity). This kernel and its convolution provides a macroscopic equivalence of the optical material for the quantum effects leading to the nonlinearity. For silica, these effects occur at time scales of 1–100 fs. Note that $\chi^{(3)}$ may have different resonances and dampings than $\chi^{(1)}$.

Consider a material having a single-Lorentzian dispersive susceptibility $\chi^{(1)}(t) = \chi(t)$ characterized by the Fourier transform pair

$$\chi(t) = \frac{(\varepsilon_s - \varepsilon_\infty)\omega_0^2}{\sqrt{\omega_0^2 - \delta^2}} e^{-\delta t} \sin\left(\sqrt{\omega_0^2 - \delta^2}\, t\right) U(t)$$
$$\Leftrightarrow \frac{(\varepsilon_s - \varepsilon_\infty)\omega_0^2}{\omega_0^2 + 2j\omega\delta - \omega^2} = \chi(\omega) \tag{26a}$$

$$\varepsilon_r(\omega) = \varepsilon_\infty + \frac{(\varepsilon_s - \varepsilon_\infty)\omega_0^2}{\omega_0^2 + 2j\omega\delta - \omega^2}$$

$$\text{where } \begin{cases} \omega_0 & \equiv \text{resonant frequency} \\ \delta & \equiv \text{damping constant.} \end{cases} \tag{26b}$$

Further, the material nonlinearity is assumed to be characterized by the following single time convolution for P_z^{NL} [29]:

$$P_z^{NL}(x, t) = \varepsilon_o \chi_o^{(3)} E_z(x, t) \int_{-\infty}^{\infty} g(t - \tau)[E_z(x, \tau)]^2\, d\tau \tag{27a}$$

where $\chi_o^{(3)}$ is the nonlinear coefficient. The causal response function $g(t - \tau)$ is normalized so that

$$\int_{-\infty}^{\infty} g(t)\, dt = 1. \tag{27b}$$

Equation (27) accounts for only nonresonant third-order processes, including phonon interactions and nonresonant electronic effects. To model these responses, we let

$$g(t) = \alpha\delta(t) + (1 - \alpha) g_R(t) \tag{28a}$$

where $\delta(t)$ is a Dirac delta function that models Kerr nonresonant virtual electronic transitions on the order of about 1 fs or less, and $g_R(t)$ is given by the exponential

$$g_R(t) = \left(\frac{\tau_1^2 + \tau_2^2}{\tau_1 \tau_2^2}\right) e^{-t/\tau_2} \sin\left(\frac{t}{\tau_1}\right) U(t) \tag{28b}$$

that models transient Raman scattering. Effectively, $g_R(t)$ models a single Lorentzian line centered on the optical-phonon frequency $1/\tau_1$ and having a bandwidth of $1/\tau_2$, the reciprocal phonon lifetime. Note that α parameterizes the relative strengths of the Kerr and Raman interactions.

Following [25], we now describe the system of coupled nonlinear ordinary differential equations that governs the time evolution of the polarization. Assuming zero values of the electromagnetic field and the kernel functions for $t \leq 0$, define the functions $F(t)$ and $G(t)$ as, respectively, the convolutions

$$F(t) = \varepsilon_o \int_0^t \chi^{(1)}(t - \tau) E_z(x, \tau)\, d\tau; \tag{29a}$$

$$G(t) = \varepsilon_o \int_0^t g_R(t - \tau)[E_z(x, \tau)]^2\, d\tau. \tag{29b}$$

Then, by time-differentiating F and G, it can be shown that these functions satisfy the system

$$\frac{1}{\omega_0^2}\frac{d^2F}{dt^2}+\frac{2\delta}{\omega_0^2}\frac{dF}{dt}+\left[1+\frac{\varepsilon_s-\varepsilon_\infty}{\varepsilon_\infty+\alpha\chi_o^{(3)}(E_z)^2}\right]F + \left[\frac{(\varepsilon_s-\varepsilon_\infty)(1-\alpha)\chi_o^{(3)}E_z}{\varepsilon_\infty+\alpha\chi_o^{(3)}(E_z)^2}\right]G = \left[\frac{\varepsilon_s-\varepsilon_\infty}{\varepsilon_\infty+\alpha\chi_o^{(3)}(E_z)^2}\right]D_z \tag{30a}$$

$$\frac{1}{\overline{\omega}_0^2}\frac{d^2G}{dt^2}+\frac{2\overline{\delta}}{\overline{\omega}_0^2}\frac{dG}{dt}+\left[1+\frac{(1-\alpha)\chi_o^{(3)}(E_z)^2}{\varepsilon_\infty+\alpha\chi_o^{(3)}(E_z)^2}\right]G + \left[\frac{E_z}{\varepsilon_\infty+\alpha\chi_o^{(3)}(E_z)^2}\right]F = \left[\frac{E_z}{\varepsilon_\infty+\alpha\chi_o^{(3)}(E_z)^2}\right]D_z \tag{30b}$$

where $\overline{\delta}=1/\tau_2$ and $\overline{\omega}_0^2=(1/\tau_1)^2+(1/\tau_2)^2$. Equations (30a) and (30b) are first solved simultaneously for F and G at the latest time step by using a second-order accurate finite-difference scheme (discussed below) that operates on data for the current value of D_z and previous values of D_z, E_z, F, and G. Then the latest value of E_z can be obtained via a Newton's iteration of the following equation, using the new values of D_z, F, and G:

$$E_z=\frac{D_z-F-(1-\alpha)\chi_o^{(3)}E_zG}{\varepsilon_o[\varepsilon_\infty+\alpha\chi_o^{(3)}(E_z)^2]}. \tag{31}$$

The finite-difference realization of the above is summarized in the two-step procedure that follows.

Step 1: Apply a second-order accurate central-difference scheme centered at time step n for the coupled system of (30a) and (b). Here the values of D_z and the convolution functions, F and G, at time step n are taken in a semi-implicit manner as the average of the respective values at time steps $n-1$ and $n+1$. This yields the latest values of the convolutions F^{n+1} and G^{n+1} and requires only two time levels of storage

$$\underbrace{\left[\frac{1}{\omega_0^2(\Delta t)^2}\right]}_{a_1}\cdot(F|_i^{n+1}-2F|_i^n+F|_i^{n-1})+\underbrace{\left(\frac{\delta}{\omega_0^2\Delta t}\right)}_{b_1} \cdot(F|_i^{n+1}-F|_i^{n-1})+\underbrace{\left[1+\frac{\varepsilon_s-\varepsilon_\infty}{\varepsilon_\infty+\alpha\chi_o^{(3)}(E_z|_i^n)^2}\right]}_{c_1} \cdot\frac{(F|_i^{n+1}+F|_i^{n-1})}{2}+\underbrace{\left[\frac{(\varepsilon_s-\varepsilon_\infty)(1-\alpha)\chi_o^{(3)}E_z|_i^n}{\varepsilon_\infty+\alpha\chi_o^{(3)}(E_z|_i^n)^2}\right]}_{d_1} \cdot\frac{(G|_i^{n+1}+G|_i^{n-1})}{2} =\underbrace{\left[\frac{\varepsilon_s-\varepsilon_\infty}{\varepsilon_\infty+\alpha\chi_o^{(3)}(E_z|_i^n)^2}\right]}_{e_1}\cdot\frac{(D_z|_i^{n+1}+D_z|_i^{n-1})}{2} \tag{32a}$$

$$\underbrace{\left[\frac{1}{\overline{\omega}_0^2(\Delta t)^2}\right]}_{a_2}\cdot(G|_i^{n+1}-2G|_i^n+G|_i^{n-1})+\underbrace{\left(\frac{\overline{\delta}}{\overline{\omega}_0^2\Delta t}\right)}_{b_2} \cdot(G|_i^{n+1}-G|_i^{n-1})+\underbrace{\left[1+\frac{(1-\alpha)\chi_o^{(3)}(E_z|_i^n)^2}{\varepsilon_\infty+\alpha\chi_o^{(3)}(E_z|_i^n)^2}\right]}_{c_2} \cdot\frac{(G|_i^{n+1}+G|_i^{n-1})}{2}+\underbrace{\left[\frac{E_z|_i^n}{\varepsilon_\infty+\alpha\chi_o^{(3)}(E_z|_i^n)^2}\right]}_{d_2} \cdot\frac{(F|_i^{n+1}+F|_i^{n-1})}{2} =\underbrace{\left[\frac{E_z|_i^n}{\varepsilon_\infty+\alpha\chi_o^{(3)}(E_z|_i^n)^2}\right]}_{e_2}\cdot\frac{(D_z|_i^{n+1}+D_z|_i^{n-1})}{2}. \tag{32b}$$

Upon collecting like terms and simplifying the notation as shown, we obtain the following pair of equations for the updated convolution integrals $F|_i^{n+1}$ and $G|_i^{n+1}$:

$$\left(a_1+b_1+\frac{c_1}{2}\right)F|_i^{n+1}+\left(\frac{d_1}{2}\right)G|_i^{n+1} =2a_1F|_i^n+\left(b_1-a_1-\frac{c_1}{2}\right)F|_i^{n-1} -\left(\frac{d_1}{2}\right)G|_i^{n-1}+\left(\frac{e_1}{2}\right)\cdot(D_z|_i^{n+1}+D_z|_i^{n-1}) \tag{33a}$$

$$\left(\frac{d_2}{2}\right)F|_i^{n+1}+\left(a_2+b_2+\frac{c_2}{2}\right)G|_i^{n+1} =2a_2G|_i^n+\left(b_2-a_2-\frac{c_2}{2}\right)G|_i^{n-1} -\left(\frac{d_2}{2}\right)F|_i^{n-1}+\left(\frac{e_2}{2}\right)\cdot(D_z|_i^{n+1}+D_z|_i^{n-1}). \tag{33b}$$

Note that the form of the coupling in (33a) and (33b) results in a strong diagonal dominance in the associated matrix. This feature is essential for a stable algorithm.

Step 2: Substitute the values of $D_z|_i^{n+1}$, $F|_i^{n+1}$, and $G|_i^{n+1}$ into (27) to determine $E_z|_i^{n+1}$ via a Newton iteration procedure. Suppressing the i subscript, we obtain

$$E_z^{\langle p+1\rangle}=\frac{D_z|^{n+1}-F|^{n+1}-(1-\alpha)\chi_o^{(3)}E_z^{\langle p\rangle}G|^{n+1}}{\varepsilon_o[\varepsilon_\infty+\alpha\chi_o^{(3)}(E_z^{\langle p\rangle})^2]} \qquad p=0,\,1,\,2,\,\cdots \tag{34}$$

where $E_z^{\langle p\rangle}$ denotes the approximation of $E_z|^{n+1}$ at the pth iteration of the Newton procedure and $E_z^{\langle 0\rangle}=E_z|^n$. Results to date indicate that only a single iteration of this procedure is sufficient for converged values of the electric field.

The FDTD modeling of a 50-fs pulsed optical-signal source switched on at $t=0$ at the surface $x=0$ of a material half-space having nonlinear dispersive properties was reported in [25]. The pulse was assumed to have unity amplitude of

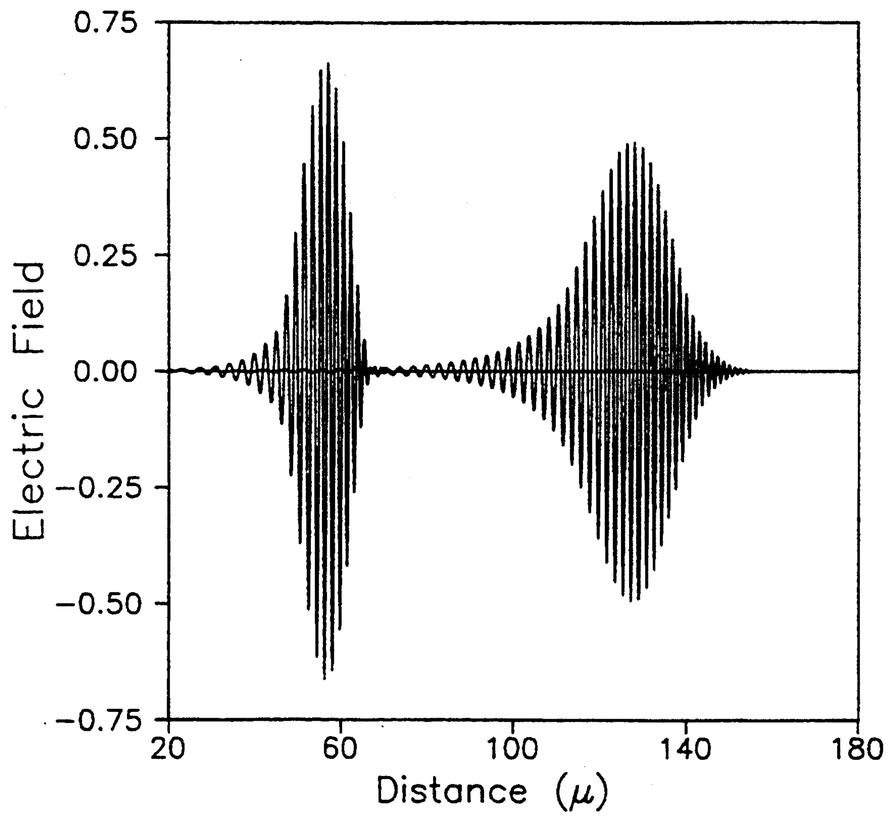

Fig. 4. (a) FDTD results for a 50-fs optical carrier pulse after propagating 55 μm and 126 μm in a Lorentz-dispersive medium (linear case), showing the attenuation, broadening, and frequency-modulation effects of anomalous dispersion. (b) Corresponding FDTD results for the nonlinear dispersive case, showing the formation of a temporal soliton and a small precursor pulse. $\Delta x = 7.299$ nm, $\Delta t = 12.16$ as. Problem size: 20 000 1-D cells, 40 000 time steps. Computer resources: 0.5 MW; 630 CPU s on a single processor of the Cray J90 [25].

its sinusoidal-carrier electric field, a carrier frequency $f_c = 1.37 \times 10^{14}$ Hz ($\lambda = 2.19\,\mu$m), and a hyperbolic secant envelope function with a characteristic time constant of 14.6 fs. Approximately seven cycles of the optical carrier were contained within the pulse envelope, and the center of the pulse coincided with a zero crossing of the sinusoid. To demonstrate soliton formation over short propagation spans of less than 200 μm, the material's group velocity dispersion, β_2, and nonlinear coefficient, $\chi_o^{(3)}$, were appropriately scaled by selecting the following parameters:

1) linear dispersion: $\varepsilon_s = 5.25$, $\varepsilon_\infty = 2.25$, $\omega_0 = 4 \times 10^{14}$ s^{-1}, $\delta = 2 \times 10^9$ s^{-1};
2) nonlinear dispersion: $\chi_o^{(3)} = 7 \times 10^{-2}$ (V/m)$^{-2}$, $\alpha = 0.7$, $\tau_1 = 12.2$ fs, $\tau_2 = 32$ fs.

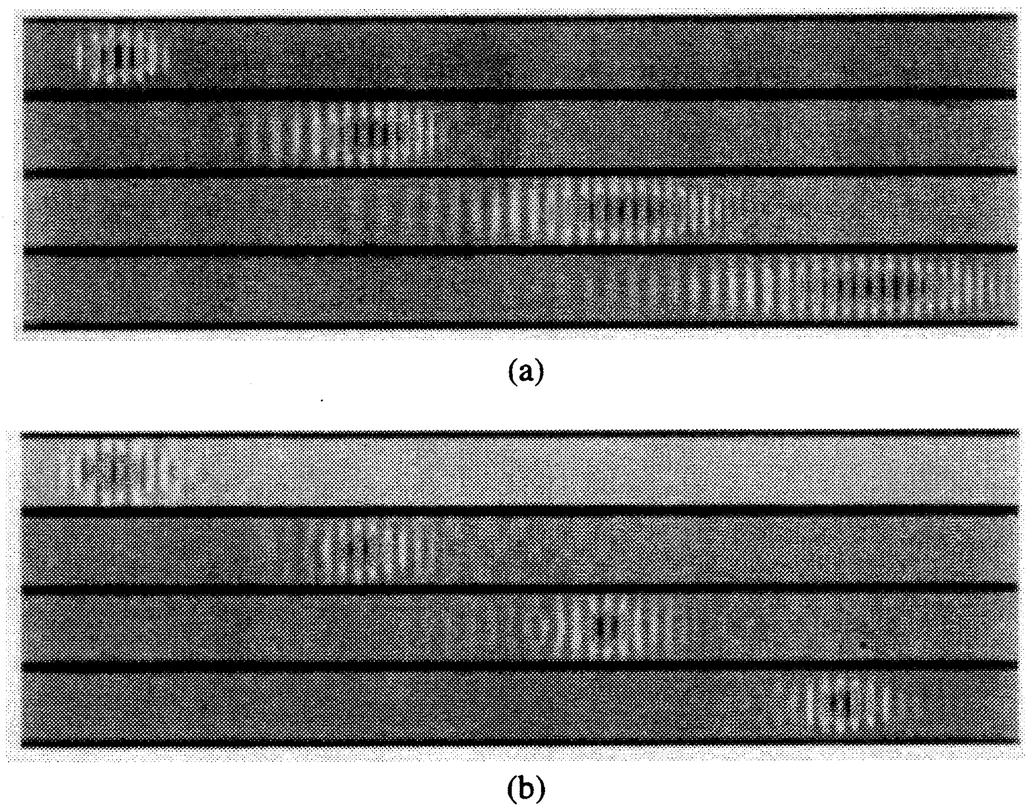

Fig. 5. Visualization of the FDTD computed electric field of a 50-fs optical carrier pulse propagating in a 1-μm thick slab waveguide. (a) Pulse spreading and frequency modulation due to anomalous linear dispersion in the slab waveguide. (b) Corresponding FDTD results for the nonlinear dispersive case showing the formation of a temporal soliton. $\Delta x = \Delta y = 43.8$ nm, $\Delta t = 72.99$ as. 13 334 time steps. Computer resources: 6.0 MW; 3100 CPU s on a single processor of the Cray J90 [26].

This choice resulted in β_2 varying in a wide range from -7 to -75 ps^2/m over the spectral width of the modeled pulse, $(1.37 \pm 0.2) \times 10^{14}$ Hz. Finally, by choosing a uniform FDTD space resolution of 7.3 nm ($\cong \lambda_o/300$), the numerical phase velocity error was limited to about 1 part in 10^5—very small compared to the physical dispersions modeled.

Fig. 4 (taken from [25]) depicts the results of the dispersive and nonlinear dispersive FDTD computations. In Fig. 4(a), the computed rightward propagating pulse for the linear Lorentz dispersive case [$\chi_o^{(3)}$ set to zero] is graphed at $n = 20\,000$ and 40 000 time steps. This corresponds to pulse propagation to depths of $x = 55\,\mu$m and 126 μm at times of 487 and 973 fs, respectively, after initiation. It is clear that the assumed linear dispersion caused substantial broadening of the computed pulse along with diminishing amplitude and carrier frequency modulation: $> f_c$ on the leading side of the pulse, and $< f_c$ on the trailing side of the pulse.

Fig. 4(b) graphs the corresponding pulse propagation when the dispersive nonlinearity was actuated. Upon the precise choice of $\chi_o^{(3)}$ and the initial pulse amplitude, this yielded a rightward propagating *temporal soliton* that retained its amplitude and width. Here, the temporal pulse width spreading effect caused by the assumed linear dispersion was exactly balanced by the temporal pulse width sharpening effect caused by the assumed nonlinearity. The smaller magnitude "daughter" pulses have been identified as transient third harmonic energy [8].

Fig. 5(a) and (b) (taken from [26]) depicts the FDTD-computed results of the 2-D versions of Fig. 4(a) and (b). Here, the pulse was assumed to have the field components E_z, H_x, and H_y and be guided in the $+x$-direction by a 1-μm thick planar dielectric slab with vacuum to either side. Again, it was found possible to obtain a propagating, nondispersing, temporal soliton by the precise choice of $\chi_o^{(3)}$ and the pulse amplitude.

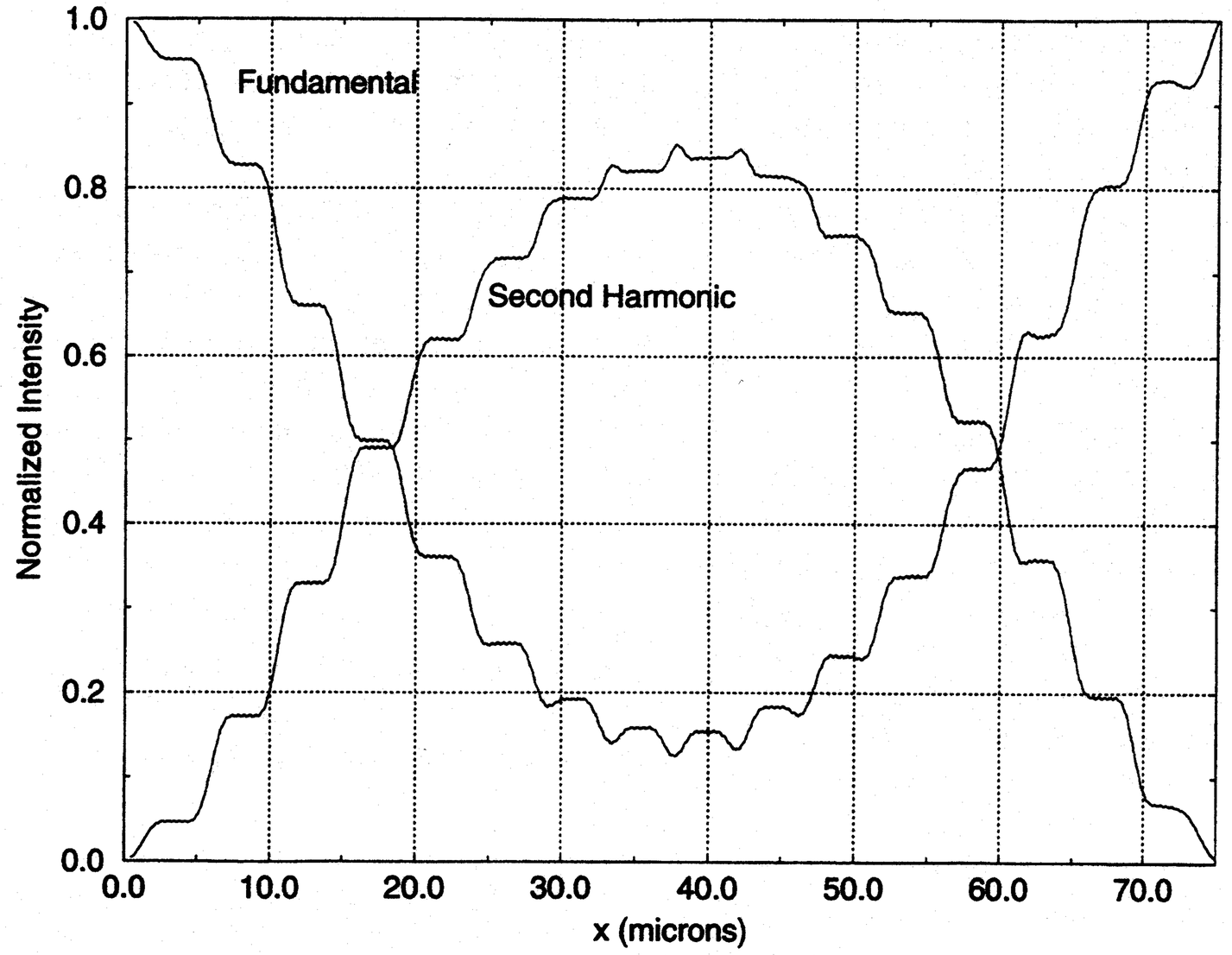

Fig. 6. FDTD-computed normalized intensities for both the fundamental ($\lambda = 1.5\,\mu$m) and the second-harmonic ($\lambda = 0.75\,\mu$m) fields along the length of a 2-D slab waveguide with a QPM grating of period 4.54 μm. $\Delta x = 20.83$ nm, $\Delta t = 34.7$ as. 10 000 time steps. Computer resources: 6.7 MW; 1300 CPU s on a single processor of the Cray J90.

IV. Second-Order Nonlinear Media

This section presents a simple FDTD algorithm to model electromagnetic wave propagation in materials exhibiting an instantaneous second-order nonlinearity. (Work is in progress to extend this approach to the case of a dispersive second-order nonlinearity.) Similar to the Kerr nonlinearity, this is modeled in the relation $D = \varepsilon_o \varepsilon E$, but now

$$\varepsilon = \varepsilon_0[n_0^2 + \chi^{(2)}E] \tag{35}$$

where the nonlinear coefficient $\chi^{(2)}$ has units of m/V. The latest value of E in (7) can be obtained by iteration, using the new value of D and the old value of E

$$E = \frac{D}{\varepsilon_0[n_0^2 + \chi^{(2)}E]}. \tag{36}$$

Knowledge of E then permits another updating of H and D, and the process repeats cyclically until time-stepping is completed.

This nonlinear FDTD model is now applied to study the well-characterized process of second-harmonic generation in a second-order nonlinear semiconductor waveguide in two dimensions. Second-harmonic generation can occur due to the interaction of an applied field at frequency f_0 with the $\chi^{(2)}$ nonlinear medium, resulting in a copropagating signal oscillating at frequency $2f_0$. Due to waveguide modal dispersion, the guided mode of the second-harmonic field travels with a speed different from that of the guided mode of the applied field. The efficiency of the frequency-conversion depends on the degree of phase matching between the two signals [5].

In the present example, an asymmetric 0.44-μm thick slab waveguide ($n = 3.1$ substrate, $n = 3.6$ guiding layer, $n = 1$ air) is excited by a CW signal at the fundamental $\lambda_0 = 1.5\,\mu$m. The waveguide is designed to support only a single mode at this frequency with a mode effective index of $n_{eff_1} = 3.400$. However, the waveguide can support at least two distinct modes at the second harmonic. The effective index for the lowest order guided mode at the second-harmonic frequency is $n_{eff_2} = 3.357$. The phase mismatch is defined as $\Delta k = 2k_0(n_{eff_2} - n_{eff_1})$. The nonlinear coefficient is $\chi^{(2)} = 300 \times 10^{-12}$ m/V, and the incident field amplitude is 1.0×10^9 V/m.

As energy at the fundamental frequency propagates down the guide, energy at the harmonic frequency is generated and begins to propagate in the same direction. Note that the process of harmonic generation occurs continuously along the entire length of the guide. For there to be an appreciable buildup of harmonic energy, the harmonic energy generated early in this process and propagating down the guide must constructively interfere with that generated later on. In a homogeneous nonlinear waveguide, low frequency-conversion efficiency occurs because the generated harmonic field gets out of phase with its driving polarization, and power flows from the harmonic field back into the fundamental.

When the condition of perfect phase matching is fulfilled, the generated wave maintains a fixed-phase relation with respect to the nonlinear polarization and is able to extract energy most efficiently from the incident wave. Quasi-phase matching (QPM) [30] is a method of effectively reducing the phase mismatch between the two fields. One approach to QPM, selective-area disordering [31], is to periodically zero

out the nonlinear coefficient along the direction of propagation by using a grating structure that combines layers of linear and nonlinear dielectric materials. Here, the second-harmonic field is allowed to grow during the nonlinear half-period of the grating but remains steady during the linear half-period, whereas in a bulk nonlinear medium it would have continued to develop out of phase. This results in a stepwise increase of the second-harmonic field and a corresponding stepwise decrease of the fundamental field.

In the present example, the period of the QPM grating is $\Lambda = 4.54\,\mu$m. Although the guide can support more than one mode at the harmonic frequency, this choice of grating period ensures that only the lowest order mode propagates. Fig. 6 shows the intensity of both the fundamental and harmonic fields along the length of the waveguide. The bilateral exchange of energy from the fundamental to the harmonic and back to the fundamental is evident. Simply by truncating the waveguide at 40 μm, it is possible to maximize the transfer of energy to the harmonic.

Since this particular problem involves paraxial wave propagation, other less computationally intensive approaches such as the beam propagation method (BPM) [30], [32] are appropriate and, in fact, offer advantages relative to waveguide length and dimensionality. While the full power of the FDTD Maxwell's equations solver may not be required for this example, it is easy to see how a variety of engineered structural features in this and similar nonlinear optical devices could violate the paraxial assumptions. What has been shown is that FDTD can readily model the physics of instantaneous second-order optical nonlinearities. Work is ongoing to construct a comprehensive validation versus BPM and to investigate numerical stability issues.

V. Conclusion

This paper summarized algorithms which extend the FDTD Maxwell's equations approach to nonlinear optics. The use of FDTD in this field is novel. Previous analytical and numerical methods such as the NLSE and the BPM were aimed at modeling optical-wave propagation in electrically long structures such as glass fibers and directional couplers, wherein the primary flow of energy is along a single principal direction. FDTD approaches, however, are aimed primarily at modeling compact optical structures spanning in the order of the wavelength of light and having energy flow in arbitrary directions.

Relative to NLSE and BPM, FDTD is certainly very computationally intensive. However, it has the advantage of being substantially more robust than either NLSE or BPM because it directly solves for fundamental quantities, the optical E and H fields in space and time. FDTD avoids the simplifying assumptions that lead to conventional asymptotic and paraxial-propagation analyses. It rigorously enforces the vector field boundary conditions at all material interfaces at the time scale of a small fraction of the optical period, whether or not the media are dispersive or nonlinear.

For all of the third-order nonlinear cases presented here, the time step was chosen to be at or just below the Courant stability limit. No stability problems were observed, even after several hundred thousand time steps. Numerical stability issues for the second-order nonlinear algorithm are being investigated.

Extending the FDTD algorithm to the field of active nonlinear optics is an area of current research. It is now possible to model the electrodynamics of micron-scale laser cavities in two and three dimensions, using algorithms for the macroscopic effects of optical-gain media [33], [34]. An emerging frontier is the combination of FDTD classical electrodynamics and the quantum mechanics of the materials being modeled [35].

Acknowledgment

The authors would like to thank P. M. Goorjian of NASA-Ames Research Center, Moffett Field, CA, for his collaboration in the development of the nonlinear dispersive algorithm.

References

[1] K. S. Yee, "Numerical solution of initial boundary value problems involving Maxwell's equations in isotropic media," *IEEE Trans. Antennas Propagat.*, vol. AP-14, pp. 302–307, May 1966.
[2] A. Taflove, *Computational Electrodynamics: The Finite-Difference Time-Domain Method.* Norwood, MA: Artech House, 1995.
[3] K. S. Kunz and R. J. Luebbers, *The Finite Difference Time Domain Method for Electromagnetics.* Boca Raton, FL: CRC, 1993.
[4] P. N. Butcher and D. Cotter, *The Elements of Nonlinear Optics.* Cambridge, UK: Cambridge Univ. Press, 1990.
[5] R. W. Boyd, *Nonlinear Optics.* Boston, MA: Academic, 1992.
[6] G. P. Agrawal, *Nonlinear Fiber Optics.* New York: Academic, 1989.
[7] A. Hasagawa and F. Tappert, "Transmission of stationary nonlinear optical pulses in dispersive dielectric fibers I: Anomalous dispersion," *Appl. Phys. Lett.*, vol. 23, pp. 142–144, Aug. 1973.
[8] C. V. Hile and W. L. Kath, "Numerical solutions of Maxwell's equations for nonlinear optical pulse propagation," *J. Opt. Soc. Amer. B*, vol. 13, pp. 1135–1145, June 1996.
[9] M. Lax, W. H. Louisell, and W. B. McKnight, "From Maxwell to paraxial wave optics," *Phys. Rev. A*, vol. 11, p. 1365, Aug. 1975.
[10] R. Luebbers, F. P. Hunsberger, K. S. Kunz, R. B. Standler, and M. Schneider, "A frequency-dependent finite-difference time-domain formulation for dispersive materials," *IEEE Trans. Electromagn. Compat.*, vol. 32, pp. 222–227, Aug. 1990.
[11] R. J. Luebbers, F. P. Hunsberger, and K. S. Kunz, "A frequency-dependent finite-difference time-domain formulation for transient propagation in plasma," *IEEE Trans. Antennas Propagat.*, vol. 39, pp. 29–34, Jan. 1991.
[12] R. J. Luebbers and F. P. Hunsberger, "FDTD for Nth-order dispersive media," *IEEE Trans. Antennas Propagat.*, vol. 40, pp. 1297–1301, Nov. 1992.
[13] T. Kashiwa, N. Yoshida, and I. Fukai, "A treatment by the finite-difference time-domain method of the dispersive characteristics associated with orientation polarization," *Inst. Electron. Inform. Communicat. Eng. (Japan) Trans.*, vol. E-73, pp. 1326–1328, Aug. 1990.
[14] T. Kashiwa and I. Fukai, "A treatment by the FD-TD method of the dispersive characteristics associated with electronic polarization," *Microwave Opt. Tech. Lett.*, vol. 3, pp. 203–205, June 1990.
[15] R. M. Joseph, S. C. Hagness, and A. Taflove, "Direct time integration of Maxwell's equations in linear dispersive media with absorption for scattering and propagation of femtosecond electromagnetic pulses," *Opt. Lett.*, vol. 16, pp. 1412–1414, Sept. 1991.
[16] A. Sommerfeld, "Über die fortpflanzung des lichtes in disperdierenden medien," *Ann. Phys.*, vol. 44, pp. 177–202, 1914.
[17] L. Brillouin, "Über die fortpflanzung des lichtes in disperdierenden medien," *Ann Phys.*, vol. 44, pp. 203–240, 1914.
[18] K. E. Oughstun and G. C. Sherman, "Uniform asymptotic description of electromagnetic pulse propagation in a linear dispersive medium with absorption (the Lorentz medium)," *J. Opt. Soc. Amer. A*, vol. 6, pp. 1394–1420, Sept. 1989.
[19] P. Wyns, D. P. Foty, and K. E. Oughstun, "Numerical analysis of the precursor fields in linear dispersive pulse propagation," *J. Opt. Soc. Amer. A*, vol. 6, pp. 1421–1429, Sept. 1989.

[20] J. D. Jackson, *Classical Electrodynamics*, 2nd ed. New York: Wiley, 1975.
[21] R. M. Joseph and A. Taflove, "Spatial soliton deflection mechanism indicated by FDTD Maxwell's equations modeling," *IEEE Photon. Tech. Lett.*, vol. 6, pp. 1251–1254, Oct. 1994.
[22] J. S. Aitchison, A. M. Weiner, Y. Silberberg, D. E. Leaird, M. K. Oliver, J. L. Jackel, and P. W. E. Smith, "Experimental observation of spatial soliton interactions," *Opt. Lett.*, vol. 16, pp. 15–17, Jan. 1991.
[23] C. Desem and P. L. Chu, "Reducing soliton interaction in single-mode optical fibers," *Inst. Elect. Eng. Proc.*, vol. 134, pp. 145–151, June 1987.
[24] R. W. Ziolkowski and J. B. Judkins, "Nonlinear finite-difference time-domain modeling of linear and nonlinear corrugated waveguides," *J. Opt. Soc. Amer. B*, vol. 11, pp. 1565–1575, Sept. 1994.
[25] P. M. Goorjian, A. Taflove, R. M. Joseph, and S. C. Hagness, "Computational modeling of femtosecond optical solitons from Maxwell's equations," *IEEE J. Quantum Electron.*, vol. 28, pp. 2416–2422, Oct. 1992.
[26] R. M. Joseph, P. M. Goorjian, and A. Taflove, "Direct time integration of Maxwell's equations in 2-D dielectric waveguides for propagation and scattering of femtosecond electromagnetic solitons," *Opt. Lett.*, vol. 18, pp. 491–493, Apr. 1993.
[27] R. W. Ziolkowski and J. B. Judkins, "Applications of the nonlinear finite difference time domain (NL-FDTD) method to pulse propagation in nonlinear media: Self-focusing and linear/nonlinear interfaces," *Radio Sci.*, vol. 28, pp. 901–911, May 1993.
[28] ———, "Full-wave vector Maxwell equations modeling of self-focusing of ultra-short optical pulses in a nonlinear Kerr medium exhibiting a finite response time," *J. Opt. Soc. Amer. B*, vol. 10, pp. 186–198, Feb. 1993.
[29] K. Blow and D. Wood, "Theoretical description of transient stimulated Raman scattering in optical fibers," *IEEE J. Quantum Electron.*, vol. 25, pp. 2665–2673, Dec. 1989.
[30] H. M. Masoudi and J. M. Arnold, "Modeling second-order nonlinear effects in optical waveguides using a parallel processing beam propagation method," *IEEE J. Quantum Electron.*, vol. 31, pp. 2107–2113, Dec. 1995.
[31] M. M. Fejer, G. A. Magel, D. H. Jundt, and R. L. Byer, "Quasiphase-matched second-harmonic generation: Tuning and tolerances," *IEEE J. Quantum Electron.*, vol. 28, pp. 2631–2654, Nov. 1992.
[32] D. Yevick, "A guide to electric field propagation techniques for guided wave optics," *Opt. Quantum Electron.*, vol. 26, pp. 185–197, Mar. 1994.
[33] R. J. Hawkins and J. S. Kallman, "Lasing in tilted-waveguide semiconductor laser amplifiers," *Opt. Quantum Electron.*, vol. 26, pp. S207–S217, Mar. 1994.
[34] S. C. Hagness, R. M. Joseph, and A. Taflove, "Subpicosecond electrodynamics of distributed Bragg reflector microlasers: Results from finite difference time domain simulations," *Radio Sci.*, vol. 31, pp. 931–941, July/Aug. 1996.
[35] R. W. Ziolkowski, J. M. Arnold, and D. M. Gogny, "Ultrafast pulse interactions with two-level atoms," *Phys. Rev. A*, vol. 52, pp. 3082–3094, Oct. 1995.

Rose M. Joseph (M'93) was born in Kerala, India, on September 25, 1964. She received the B.S. degree in electrical engineering from the Massachusetts Institute of Technology (MIT), Cambridge, MA, in 1986, and the M.S. and Ph.D. degrees in electrical engineering from Northwestern University, Evanston, IL, in 1990 and 1993, respectively.

From 1986 to 1988, she was employed by IBM, Kingston, NY, as a Power Systems Engineer. From 1995 to 1997 she was a member of the Research Staff at the Xerox Corporation Wilson Center for Research and Technology, Webster, NY. In April 1997 she joined the technical staff at MIT Lincoln Laboratory, Lexington, MA. Her research interests include computational electromagnetics and nonlinear optics.

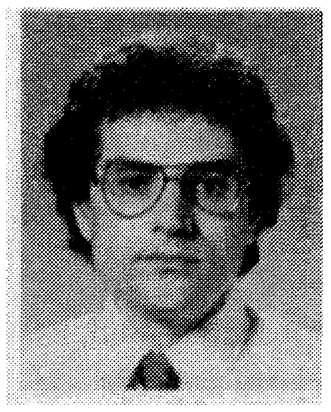

Allen Taflove (F'90) was born in Chicago, IL, on June 14, 1949. He received the B.S., M.S., and Ph.D. degrees in electrical engineering from Northwestern University, Evanston, IL, in 1971, 1972, and 1975, respectively.

Since 1988, he has been a Professor in the Department of Electrical and Computer Engineering, McCormick School of Engineering, Northwestern University, Evanston, IL. Since 1990 he has given 60 invited talks and lectures on FDTD and horizons in computational electromagnetics, in the United States and abroad, including the 90-minute keynote speech at the 1994 Salishan Meeting on High Performance Computing. He authored the textbook/research book, *Computational Electrodynamics: The Finite-Difference Time-Domain Method*, (Norwood, MA: Artech House, 1995). He originated several innovative programs in the McCormick School, including the Honors Program in Undergraduate Research (a combined B.S./Ph.D. engineering degree) and the Undergraduate Design Competition. His current research interests include FDTD simulation of picosecond-regime optical phenomena and devices, especially microlasers (in collaboration with Prof. S. T. Ho), noninvasive microwave detection and imaging of breast cancers (in collaboration with Mr. J. E. Bridges), and radio wave propagation in urban microcells (in collaboration with Mr. G. F. Stratis).

Dr. Taflove was named a Distinguished National Lecturer for the IEEE Antennas and Propagation Society in 1990–1991, and in 1992 was Chairman of the Technical Program of the IEEE Antennas and Propagation Society International Symposium in Chicago, IL. In 1991, he was named McCormick Faculty Adviser of the Year. He is a member of Eta Kappa Nu, Tau Beta Pi, Sigma Xi, International Union of Radio Science (URSI) Commissions B, D, and K, the Electromagnetics Academy, AAAS, and New York Academy of Sciences. His biographical listings include *Who's Who in Engineering, Who's Who in America, Who's Who in Science and Engineering,* and *Who's Who in American Education.*